Experimental Neurology 320 (2019) 113003

Contents lists available at ScienceDirect

Experimental Neurology

journal homepage: www.elsevier.com/locate/yexnr

Research paper

Astrogliosis inhibition attenuates hydrocephalus by increasing cerebrospinal fluid reabsorption through the glymphatic system after germinal matrix hemorrhage

Yan Ding[a,1], Tongyu Zhang[a,1], Guangyong Wu[a], Devin W. McBride[a], Ningbo Xu[a], Damon W. Klebe[a], Yiting Zhang[a], Qian Li[a], Jiping Tang[a], John H. Zhang[a,b,c,*]

[a] Department of Physiology and Pharmacology, School of Medicine, Loma Linda University, Loma Linda, CA 92350, United States of America
[b] Department of Neurosurgery, Loma Linda University Medical Center, Loma Linda, CA 92350, United States of America
[c] Department of Anesthesiology, Loma Linda University Medical Center, Loma Linda, CA 92350, United States of America

ARTICLE INFO

Keywords:
Germinal matrix hemorrhage
Glymphatic system
Astrogliosis
Post-hemorrhagic hydrocephalus
Aquaporin-4

ABSTRACT

Germinal matrix hemorrhage (GMH) results from the rupture of the immature thin-walled blood vessels and consequent bleeding into the subependymal germinal matrix and possible lateral ventricles. The purpose of this study is to investigate how astrogliosis impacts the glymphatic-meningeal lymphatic system in cerebrospinal fluid (CSF) reabsorption after GMH and how the anti-scarring agent olomoucine attenuates post-hemorrhagic hydrocephalus. GMH was induced by stereotaxic collagenase infusion into P7 Sprague-Dawley rats of both sexes. Western blot and immunofluorescence were used to assess astrogliosis and how astrogliosis affects glymphatic function by measuring Aquaporin-4 expression. Intracisternal injection of fluorescence tracer was used to measure CSF diffusion throughout the brain, its dispersion in the paravascular area and CSF drainage into the deep cervical lymph nodes at 28 days after GMH. Both short-term and long-term behavioral tests were used to assess the neurological outcomes. Nissl staining was used to assess the morphological changes at 28 days after hemorrhage. GMH elicited astrogliotic scarring and reduced the exchange between CSF and interstitial fluid, as well as CSF reabsorption through the meningeal lymphatic vessels. This might be associated with redistribution of Aquaporin-4. Olomoucine ameliorated scar tissue formation and attenuated post-hemorrhagic hydrocephalus. These findings of this study suggested that the glymphatic system might play a role in CSF reabsorption in neonates following GMH. Scar tissue formation impairs this CSF clearance route, and therefore astrogliosis inhibition might be a potential therapeutic strategy for neonatal post-hemorrhagic hydrocephalus.

1. Introduction

Germinal matrix hemorrhage (GMH) results from rupture of the thin-walled vessels in the germinal matrix of preterm infants. GMH can lead to devastating consequences, such as post-hemorrhagic hydrocephalus (PHH) (Ballabh, 2010; Ballabh et al., 2004). The only effective treatment available to treat PHH is surgical shunting, but post-surgical shunting complications and chronic obstruction are problematic and costly.

Cerebrospinal fluid (CSF), secreted primarily from the choroid plexus, travels through the cerebroventricular system by pulsatile bulk flow and gets reabsorbed through the subarachnoid villi. In neonates, however, the subarachnoid villi are underdeveloped and sparsely distributed (Johnston, 2003; Zakharov et al., 2003). This leads to the speculation that the newly-identified "glymphatic system" might play a greater role in neonates. The glymphatic system functions in a manner similar to conventional lymphatics in that it contains analogous paravascular channels where CSF exchanges waste for elimination with the interstitial fluid (ISF). Three key components make up the glymphatic system: para-arterial CSF influx, astrocytic aquaporin-4 (AQP4) and para-venous clearance (Iliff et al., 2012). A previous report has shown that ISF clearance was reduced by 70% in AQP4 knockout mice (Iliff

Abbreviations: AQP4, Aquaporin-4; CDK, Cyclin-Dependent Kinase; CSF, Cerebrospinal Fluid; dcLN, Deep Cervical Lymph Node; GMH, Germinal Matrix Hemorrhage; HDAC, Histone Deacetylase; ISF, Interstitial Fluid; PCNA, Proliferating Cell Nuclear Antigen; PHH, Post-hemorrhagic Hydrocephalus; Rb, Retinoblastoma protein; RECA-1, Rat Endothelial Cell Antigen-1

* Corresponding author at: Risley Hall, 11041 Campus St, Loma Linda, CA 92350, United States of America.
E-mail address: johnzhang3910@yahoo.com (J.H. Zhang).

[1] Authors contributed equally to this work.

https://doi.org/10.1016/j.expneurol.2019.113003
Received 12 February 2019; Received in revised form 3 May 2019; Accepted 27 June 2019
Available online 28 June 2019
0014-4886/

et al., 2012). In addition, two recent reports identified the lymphatic vascular system in the meningeal compartment that ultimately drains in to the deep cervical lymph nodes (dcLNs) (Aspelund et al., 2015; Louveau et al., 2015). Although still controversial and largely unknown, the dural lymphatic vessel system might function as the downstream outflow of the glymphatic system for the clearance of molecules (Louveau et al., 2017; Sun et al., 2018).

Although neonatal astrocytes demonstrate greater plasticity than those in adults, previous reports from our laboratory demonstrate that GMH elicits significant inflammatory response and astrogliosis, as shown by increased GFAP level, which sustains for up to 28 days after the hemorrhage (Balasingam et al., 1994; Lekic et al., 2012; Manaenko et al., 2014). Astrogliotic scarring is associated with ventricular dilation and decreased scar tissue formation correlates with reduced ventriculomegaly after GMH (Manaenko et al., 2014). However, the underlying mechanisms remain largely unknown. Previous studies suggest that astrogliosis affects the glymphatic system by altering AQP4 expression and polarity in both ischemic stroke and traumatic brain injury (Iliff and Nedergaard, 2013; Wang et al., 2012). Thus, it would be intriguing to verify if this also holds true in neonates after GMH.

Olomoucine is a cyclin-dependent kinase (CDK) inhibitor. In vitro studies have shown that olomoucine targets the Cyclin E-CDK2 complex to prevent DNA acetylation when the cells are going under G1-S phase (Raynaud et al., 2005). It has been shown to be protective in several central nervous system injuries with the mechanisms related with astrogliosis inhibition (Di Giovanni et al., 2005; Tian et al., 2006; Zhu et al., 2007).

Thus, in this present study, we hypothesize that GMH-induced astrogliosis decreases CSF transport through the glymphatic system via AQP-4 redistribution leading to hydrocephalus and ventriculomegaly. We further hypothesize that olomoucine will attenuate hydrocephalus and ventriculomegaly by reducing astrogliosis, which might be associated with preventing AQP-4 redistribution.

2. Materials and methods

The data that support the findings of this study are available from the corresponding author, who is responsible for maintaining availability, upon request.

2.1. Animals and surgeries

All experiments protocols and procedures were approved by the Institutional Animal Care and Use Committee at Loma Linda University. All studies were conducted in accordance with the National Institutes of Health Guide for the Care and Use of Laboratory Animals (NIH Publications No. 8023, revised 1978). Animal studies were reported according to ARRIVE guidelines. A total of one hundred and fifty-five pups were used, of which two died during the operations. P7 Sprague-Dawley rats of both sexes were purchased from Envigo (Livermore, CA). GMH was induced as previously described (Feng et al., 2017). Briefly, animals were anesthetized with 3% isoflurane and placed onto stereotaxic frame. Isoflurane concentration was then reduced to 2%. After the scalp area was disinfected, Bregma was exposed. A 1 mm burr hole at the following stereotactic coordinates was drilled: 1.6 mm (rostral) and 1.5 mm (lateral, right). A 27-gauge needle was inserted to a depth of 2.7 mm from the dura. Using a microinfusion pump (Harvard Apparatus, Holliston, MA), 0.3 U of clostridial collagenase VII-S (Sigma-Aldrich) in 3 μL was infused through the Hamilton syringe at the rate of 1 μL/min. The needle remained in place for an additional 5 min after injection to prevent leakage. The needle was then withdrawn at the rate of 0.5 mm/min, the burr hole was sealed with bone wax and the incision was sutured. Pups were allowed to recover on a 37 °C heated blanket. Upon the recovery from anesthesia, the animals were returned to their dams. Sham-operated animals were subjected to needle insertion alone without collagenase infusion.

2.2. Drug administration

Olomoucine (Abcam) was administered at 1 h post-ictus at the dose of 1 mg/kg, 3 mg/kg or 9 mg/kg (i.p.) for three consecutive days for the three-day studies. For the 28-day studies, olomoucine (3 mg/kg, i.p.) was administered for five consecutive days. EX527 (Cayman Chemical), a SIRT1 inhibitor, was administered at the dose of 10 mg/kg (i.p.) with olomoucine for three consecutive days. 5% DMSO in sterile saline was the vehicle.

2.3. Neurobehavioral tests

Short-term neurobehavioral tests include negative geotaxis and right reflex. Both were performed on Day 3 after GMH. Negative geotaxis was performed by placing a pup on a 45 degree incline with its head down and recording the time it took for the pup to make a 180 degree turn. Righting reflex was performed by placing a pup on its back position and recording the time it took for the pup to right itself. These two tests are sensitive in evaluating the developmental profile in neonates.

To assess long-term neurological function, Morris water maze and Rotorod were performed between Day 22 and Day 27 after GMH. They tested cognitive function and motor function, respectively. Morris water maze was performed as previously described (Wan et al., 2018). After the training block, animals went under 4 blocks to find the platform. The time it took for them to find the platform was recorded. At the end of the memory blocks, a probe trial was conducted with the platform removed to measure the percentage of time they spent in the quadrant where the platform was located. Rotorod was used to test the animal's ability to remain on an accelerating rod. The animal's falling latency was recorded. All the neurobehavioral tests were conducted in a blinded fashion with animals coded by numbers. After the data was analyzed, the treatment groups were uncoded.

2.4. Immunofluorescence

Immunofluorescence was performed as previously described (Lu et al., 2019). Animals were anesthetized with 5% isoflurane and transcardially perfused with PBS followed by 4% formalin. After brains were removed, they were stored in 4% formalin at 4 °C overnight and transferred to 30% sucrose for 3–5 days until they sank to the bottom. Brains were embedded in Optimal Cutting Temperature (OCT) and frozen at −80 °C until they were sectioned. Eight micrometer-thick coronal sections were obtained using a cryostat (Leica). After sections were permeablized with 0.3% Triton-100× and blocked with 5% donkey serum, they were incubated with primary antibodies overnight. Appropriate secondary antibodies (Jackson ImmunoResearch) were diluted to 1:200 and incubated for 2 h at room temperature. Sections were mounted with PROLONG anti-fading media with DAPI (Vector Laboratories) and visualized using a microscope (Leica). Primary antibodies were anti-GFAP (Abcam, ab16997), anti-AQP4 (Santa Cruz Biotechnology, sc-9888), and anti-RECA-1 (Santa Cruz Biotechnology, sc-52665). Immunofluorescence intensity was measured using ImageJ (NIH). For AQP-4 measurement, AQP-4 was categorized into “paravascular” and “stromal” subtypes. We measured the fluorescence intensity for each AQP-4 and averaged them out for both categories. For cell counting, three areas were chosen in the periventricular area for imaging. Cells were counted in each image and cell numbers were averaged for each animal.

2.5. CSF dynamics measurement

Animals were anesthetized intraperitoneally with a mixture of ketamine (80 mg/kg) and xylazine (20 mg/kg) until no pinch-paw reflex was observed. Anesthetized animals were fixed in a stereotaxic frame and a Hamilton syringe with a 30GA needle was inserted into the

cisterna magna. Fluorescence tracer tetramethylrhodamine-dextran-3 (TR-3; molecular size 3kD; ThermoFisher) was reconstituted in artificial cerebrospinal fluid (aCSF) at a concentration of 0.25% and a total volume of 45 μL was injected into the cisterna magna at the rate of 1.6 μL/min(Yang et al., 2013). 20 min after the infusion was finished, the deep cervical lymph nodes (dcLNs) were isolated. Animals were perfused with 4% formalin transcardially and brains were removed. The brains and dcLNs were incubated in 4% formalin overnight and transferred to 30% sucrose for another 3–4 days. Brains and dcLNs were then embedded in OCT and stored at −80 °C until sectioning. 10 μm coronal sections of the brains and dcLNs were collected with a cryostat (Leica) and visualized with fluorescence microscope (Leica). Fluorescence intensity was quantified using ImageJ (NIH).

The same tracer injection procedure was performed on another set of animals. Immediately after the injection, brains were removed and imaged using a two-photon microscope (Zeiss LSM 710 NLO). Two to three cortical arteries in the injured hemisphere were located in each brain and the paravascular area was imaged to evaluate tracer dispersion. For each vessel, three or four regions of interest (ROIs) were chosen randomly for fluorescence intensity measurement. Intensity was quantified in ImageJ (NIH).

2.6. Histological volumetric study

28 days after GMH, animals were sacrificed, and brains were collected. Nissl staining was performed as previously described (Manaenko et al., 2014). Optical dissector principles were used to delineate cerebral structure borders following previously defined criteria from stereologic neuroanatomical studies. Volumes were calculated as the average delineated area from 10 μm sections taken approximately at 1.70 mm and 0.70 mm rostral to Bregma, and 1.88 mm and 3.30 mm caudal to Bregma(Wan et al., 2018). ImageJ (NIH) was used to analyze ventricular volume, cortical thickness and white matter area in Nissl stained histological brain sections as previously described (Klebe et al., 2014).

2.7. Western blot

For whole cell protein analysis, tissues were lysed using RIPA Lysis Buffer System (Santa Cruz Biotechnology) following the manufacturer's the instructions. For nuclear protein analysis, NE-PER Nuclear and Cytoplasmic Extraction Reagents (Thermo Scientific) were used to isolate nuclear protein lysates according to the manufacturer's instructions. Western blot was performed as previously described (Yu et al., 2018). Briefly, 30 μg protein lysates were separated by SDS-PAGE and transferred onto nitrocellulose membranes. After blocking with 5% milk for 1 h, membranes were incubated with primary antibodies at 4 °C overnight. Appropriate secondary antibodies (1:4000, Santa Cruz) were used for two-hour incubation at room temperature. Membranes were visualized by ECL plus kit (GE Healthcare and Life Science). Primary antibodies: anti-GFAP (Abcam, ab16997), anti-PCNA (Santa Cruz Biotechnology, sc-9857), anti-actin (Santa Cruz Biotechnology, sc-1616), anti-tubulin (Santa Cruz Biotechnology, sc-9104), anti-AQP4 (Santa Cruz Biotechnology, sc-9888), anti-phospho-Rb (Abcam, ab47474), anti-Rb (Santa Cruz Biotechnology, sc-102), anti-SIRT1 (Santa Cruz Biotechnology, sc-15404), anti-Cyclin E (Millipore, 07-687), anti-Cyclin D1 (Abcam, ab134175), anti-Iba-1 (Abcam, ab178847) and anti-Lamin B (Abcam, ab133741).

2.8. Rigor and statistical analysis

In this study, animals were numbered and randomly formed into different experimental groups using Excel. All the experimental groups were blinded for the surgeons and researchers who performed all outcomes and analyzed the data. Sample size was determined according to our previous publications for similar outcomes. Samples size was estimated using a type I error rate of 0.05 and a power of 0.8 on a 2-sided test by power analysis. Parametric data was analyzed was using one-way ANOVA followed by Tukey's *post-hoc* test. Longitudinal data were analyzed by two-way ANOVA with Tukey's *post-hoc* test. Data were expressed as mean ± SD. P values of < 0.05 were considered statistically significant. GraphPad Prism 6 (La Jolla, CA, USA) and SigmaPlot 11.0 (SysStat, Germany) were used for graphing and analyzing all the data.

3. Results

3.1. Olomoucine improved short-term neurobehavior and attenuated astrocytic proliferation at 3 days after GMH

GMH impaired short-term neurological function, as demonstrated in negative geotaxis and right reflex tests. We administered three doses of olomoucine: 1 mg/kg, i.p. (low dose), 3 mg/kg, i.p. (medium dose) and 9 mg/kg, i.p. (high dose). Both medium and high doses of the treatment improved short-term neurological performance significantly compared to the vehicle-treated group. Low dose treatment partially exerted beneficial effects in these two tests. However, they were not significant from the vehicle group (Fig. 1A and B). To avoid potential toxic effects from high dosage, we chose to use the medium dose for the remainder of the studies.

Olomoucine is a CDK inhibitor that arrests cell cycle mainly at the G1-S stage. The proliferating cell nuclear antigen (PCNA) is a cell proliferation marker at this stage. Several studies have shown that it effectively inhibits astrogliosis after CNS injuries (Di Giovanni et al., 2005; Tian et al., 2006; Zhu et al., 2007). To verify its effect in the context of GMH, we performed Western blot for the astrocyte marker GFAP and PCNA at 3 days after GMH. The results showed that GMH elicited proliferation of astrocytes at three days after the hemorrhage, as shown by higher expression levels of both GFAP and PCNA. Olomoucine effectively attenuated the induction of GFAP and PCNA compared to the vehicle-treated group (Fig. 1C–E).

To confirm that olomoucine, as a CDK inhibitor, did not affect normal neurological function in neonates at this treatment regimen, we administered olomoucine (3 mg/kg, i.p.) for three consecutive days to naïve pups that did not go under GMH. Short-term neurobehavioral tests were performed on P8 pups for three days and the results were compared with naïve pups that did not receive the treatment. Our data indicated that olomoucine alone at the dose of 3 mg/kg did not alter the neurological function during this time window. We also performed long-term neurobehavioral tests, namely Morris water maze and rotorod. Results indicated that olomoucine at this dose did not change long-term neurological outcomes compared to naïve animals (Supplemental Fig. 1). Thus, this treatment regimen was chosen for the following studies.

3.2. Olomoucine effectively attenuated astrogliosis on Day 28 after GMH

We then chose 28 days post-ictus, when the hematoma was completely cleared, to study the sustaining effect of astrogliosis. Western blot results showed that the GFAP level of the whole brain was significantly higher at 28 days after GMH and the increased GFAP expression was effectively attenuated by olomoucine treatment (Fig. 2A and B). Astrogliosis was also assessed by GFAP staining in the periventricular area, where the hematoma used to be. The number of GFAP-positive cells was significantly higher in the vehicle-treated group than the sham group. Olomoucine treatment significantly ameliorated the increase in the number of GFAP-positive cells (Fig. 2C and D).

3.3. AQP4 redistribution at 28 days after GMH

We then assessed how GMH altered the expression and localization of AQP4, a critical element of the glymphatic system for aiding in CSF

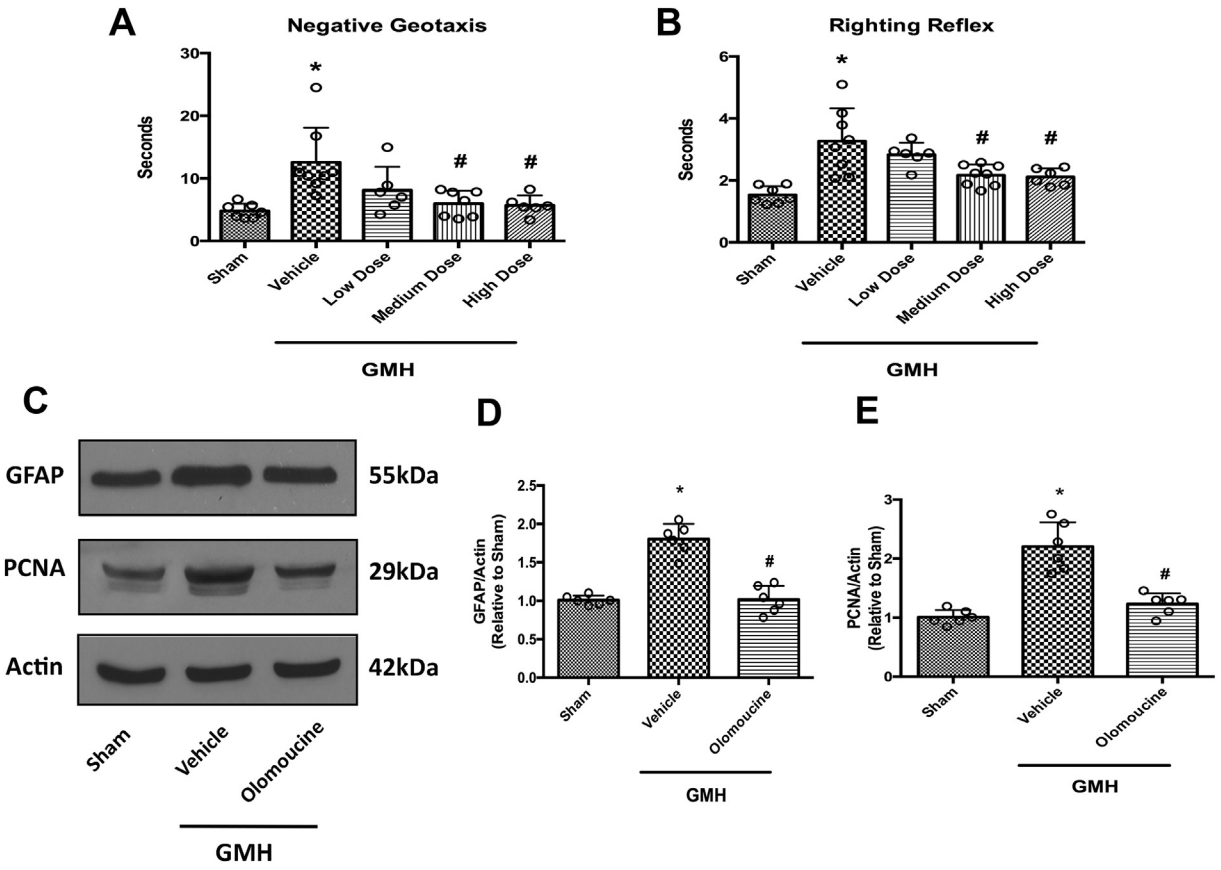

Fig. 1. Olomoucine improved short-term neurobehavioral outcomes and attenuated astrocyte proliferation at 3 days after GMH. A. Negative geotaxis at 3 days after GMH (N = 6–8). B. Righting reflex at 3 days after GMH (N = 6–8). C. Representative blots of GFAP, PCNA and actin. D. Quantitation of the densitometry of GFAP (N = 6). E. Quantitation of the densitometry of PCNA (N = 6). Values are expressed as mean ± SD. One-way ANOVA with Tukey's *post-hoc* test. $^{*}P < .05$ compared with Sham, $^{\#}P < .05$ compared with GMH + Vehicle.

movement from the para-arterial to the para-venous spaces. AQP4 is usually upregulated and contributes to edema in the acute phase after brain injuries(Fukuda and Badaut, 2012; Zador et al., 2009). However, at 28 days after GMH, AQP4 expression in the whole brain was not changed between sham and GMH animals as measured by Western blot (Fig. 3A). As shown in Supplemental Fig. 2, AQP4 was primarily expressed on astrocytes at 28 days after GMH. Immunofluorescence was performed to further distinguish paravascular AQP4 from stromal AQP4. Blood vessels were stained with the endothelial marker, Rat Endothelial Cell Antigen-1 (RECA-1) and AQP4 was stained with an antibody for AQP4. AQP4 localizing within 15 μm of a blood vessel was categorized as "paravascular" AQP4, while "stromal" AQP4 was considered to localize > 15 μm from a blood vessel. GMH caused AQP4 to be redistributed from the paravascular to the stromal space, as measured by the AQP4 fluorescence intensity. The treatment with olomoucine reversed the redistribution of AQP4; greater paravascular AQP4 and reduced stromal AQP4 was observed after olomoucine treatment (Fig. 3B and C). In summary, even though the overall AQP4 level was unchanged at 28 days after GMH, paravascular and stromal AQP4 expression levels were significantly altered.

3.4. GMH impaired CSF flow through the glymphatic system and olomoucine ameliorated the impairment

Fluorescence tracer constituted with aCSF was injected into the cisterna magna to study the CSF-ISF exchange. This tracer with the molecular weight of 3kD has been shown to diffuse easily throughout the brain parenchyma (Iliff et al., 2012). We imaged the paravascular region of the cortical arteries immediately after tracer injection. Two-photon images showed that more tracer was confined in the paravascular area and proximal brain parenchyma in the vehicle-treated group compared to the sham group, as indicated by higher fluorescence intensity. Olomoucine facilitated fluorescence tracer dispersion from the paravascular area after GMH (Fig. 4A and B).

In another set of animals, the same intracisternal injections were performed. At 20 min after the injections, coronal brain sections were obtained. The fluorescence intensity was measured throughout the whole section. Vehicle-treated animals showed significantly lower tracer diffusion, as demonstrated by lower fluorescence intensity throughout the brain. Olomoucine significantly increased the tracer diffusion compared to the vehicle group (Fig. 4C and D).

These data all suggest that GMH largely impaired CSF-ISF exchange by confining the CSF within the paravascular area and proximal brain parenchyma and that olomoucine effectively attenuated this impairment. These results were in accordance with paravascular and stromal AQP4 expression levels as shown in Fig. 3.

Two recent reports have identified the meningeal lymphatic vascular system that ultimately drains into the dcLNs. The dural lymphatic vessels function in the downstream of the glymphatic system (Aspelund et al., 2015; Louveau et al., 2015). Dissected dcLNs, from the same rats used for whole brain imaging, were imaged to verify whether there was any tracer drainage into the lymph nodes. As expected for a damaged glymphatic CSF-ISF exchange, GMH largely decreased the CSF drainage into the dcLNs, as shown by the decreased tracer inside the dcLNs. The treatment with olomoucine effectively increased the amount of CSF tracer in the dcLNs, indicating a more functional glymphatic system (i.e. more CSF reabsorption through the glymphatic-meningeal lymphatic system) (Fig. 4E and F).

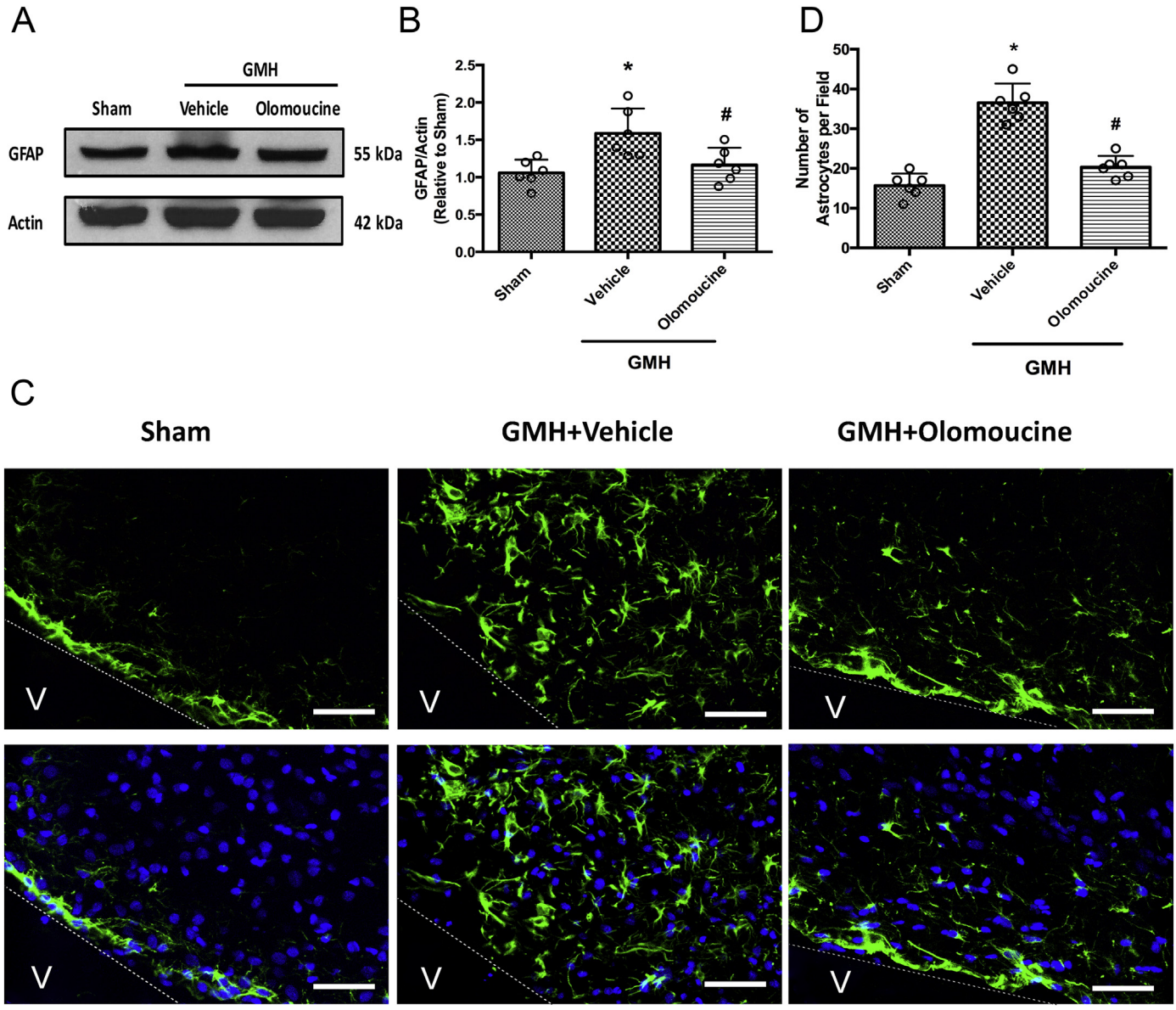

Fig. 2. Olomoucine attenuated astrogliosis at 28 days after GMH. A. Representative blots of GFAP and actin. B. Quantitation of the densitometry of GFAP over actin of each group. C. Representative images of periventricular GFAP (green) and DAPI (blue). D. Quantitation of periventricular astrocytes. Values are expressed as mean ± SD. One-way ANOVA with Tukey's *post-hoc* test. $^{*}P < .05$ compared with Sham, $^{\#}P < .05$ compared with GMH + Vehicle. N = 6. Scale bar = 50 μm. (For interpretation of the references to colour in this figure legend, the reader is referred to the web version of this article.)

3.5. Olomoucine improved long-term neurobehavioral function after GMH

In order to assess the effects olomoucine has on long-term memory and motor skills, we performed neurobehavioral tests on these animals between Day 21 and Day 26 after GMH. Morris water maze was performed and time to platform was recorded for each animal to evaluate their cognitive function. After the first day of one training block, each block was performed every day over a period of four days. Animals from different experimental groups began with comparable escape latency (Blocks 1 and 2), but by Block 3, vehicle-treated animals had a tendency to take longer time to find the platform. On Block 4, the vehicle group took significantly longer time to find the platform compared to the sham group. The olomoucine-treated group took significantly less time to find the platform compared to the vehicle group (Fig. 5A). A Probe Trial followed Block 4 to measure the percentage of the time spent in the platform quadrant with the platform removed. The vehicle-treated group spent significantly less time in the target quadrant compared to sham animals. Olomoucine-treated animals spent more time in the target quadrant compared to the vehicle group (Fig. 5B). Swimming velocity was not significantly different between groups (data not shown). Thus, the difference in latencies was due to the difference in cognitive function, rather than swimming ability.

Rotorod was performed to test the motor ability on Day 26 after GMH. Vehicle-treated animals had much shorter falling latency on accelerating rods compared to the sham group. Olomoucine treatment restored this motor function (Fig. 5C).

We also performed data analysis to see whether there was any sex difference in escape latency of Morris water maze. Data from males and females were analyzed separately. Our data showed that males and females responded similarly to GMH injury and olomoucine treatment. We did not observe differences between both sexes (Supplemental Fig. 3).

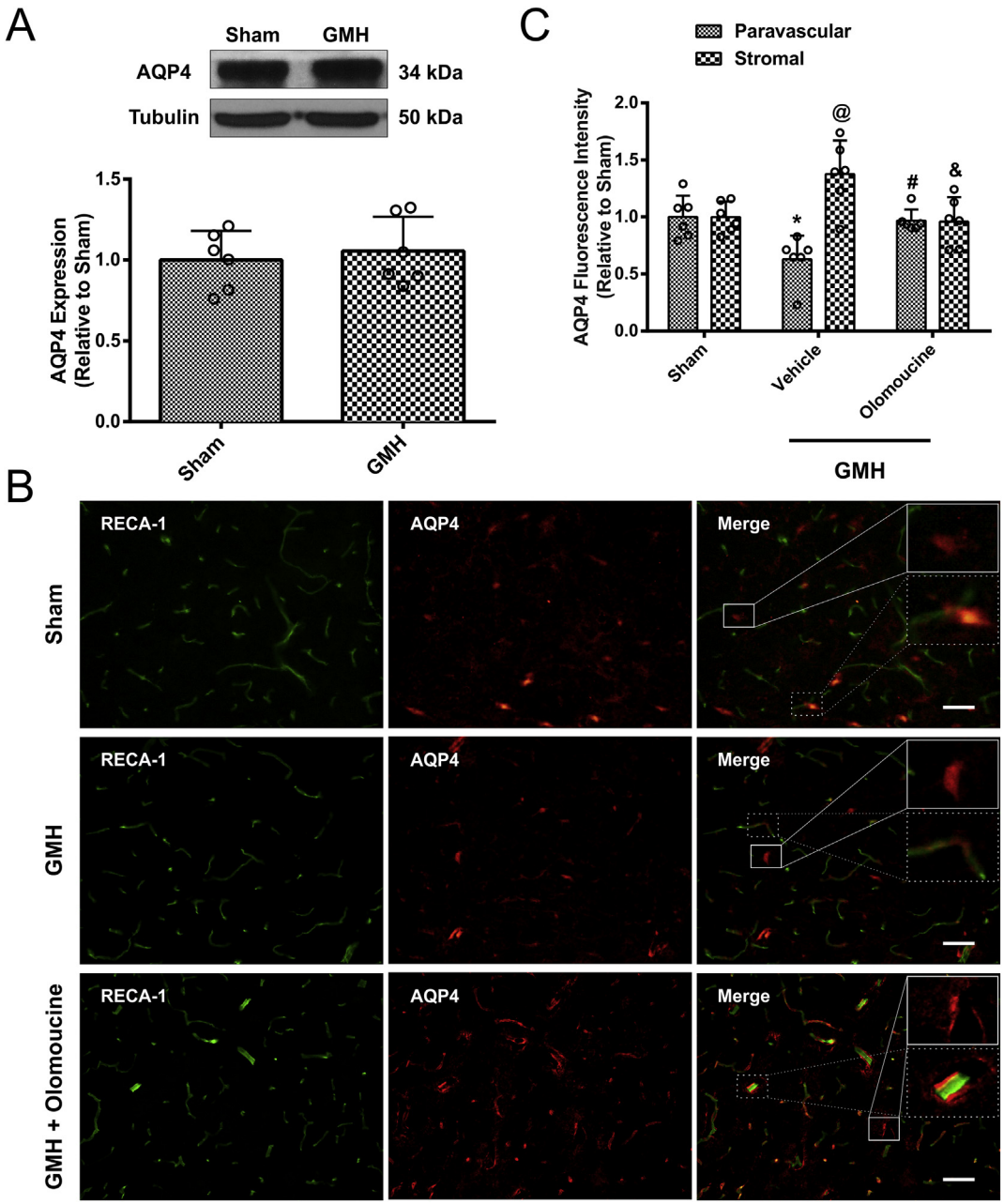

Fig. 3. AQP4 overall expression level was not altered at 28 days after GMH but it was differentially regulated. A. Representative blots of AQP4 and tubulin and quantitation of the densitometry. B. Representative images of endothelial marker RECA-1 (green) and AQP4 (red). Solid lines indicate stromal AQP4 and dash lines indicate paravascular AQP4. C. Quantitation of paravascular and stromal AQP4 fluorescence intensity. Values are expressed as mean ± SD. One-way ANOVA with Tukey's test. $^{*}P < .05$ compared with paravascular sham group. $^{@}P < .05$ compared with stromal sham group. $^{\#}P < .05$ compared with paravascular vehicle group. $^{\&}P < .05$ compared with paravascular vehicle group. N = 6. Scale bar = 50 μm. (For interpretation of the references to colour in this figure legend, the reader is referred to the web version of this article.)

3.6. Olomoucine attenuated ventriculomegaly and brain atrophy on Day 28 after GMH

We then assessed ventricular dilation and brain atrophy on a morphological level. Nissl staining was performed. Ventricular volume was significantly increased in the vehicle group compared to sham animals. Olomoucine treatment significantly reduced GMH-induced ventriculomegaly. Since ventricular dilation is usually accompanied with changes in other brain structures, we assessed white matter loss and cortical thickness as previously described (Klebe et al., 2014; Manaenko et al., 2014). Both parameters were normalized compared to the sham animals. GMH caused significant tissue loss in both white matter and cortex compared to the sham group. Olomoucine ameliorated the tissue loss in the treatment group. The structural change was due to post-hemorrhagic ventricular dilation (Fig. 6).

3.7. Olomoucine attenuated astrogliosis in a SIRT1-dependent manner

Previous findings also indicate that olomoucine, a CDK inhibitor, mainly arrests cell cycle at G1-S phase (Dimova and Dyson, 2005; Raynaud et al., 2005). CDK phosphorylates Retinoblastoma protein (Rb) at Serine795. Non-phosphorylated Rb attracts histone deacetylase (HDAC), such as SIRT1, and inhibits cell cycle progression while phosphorylated Rb in nucleus promotes cell cycle into the S phase.

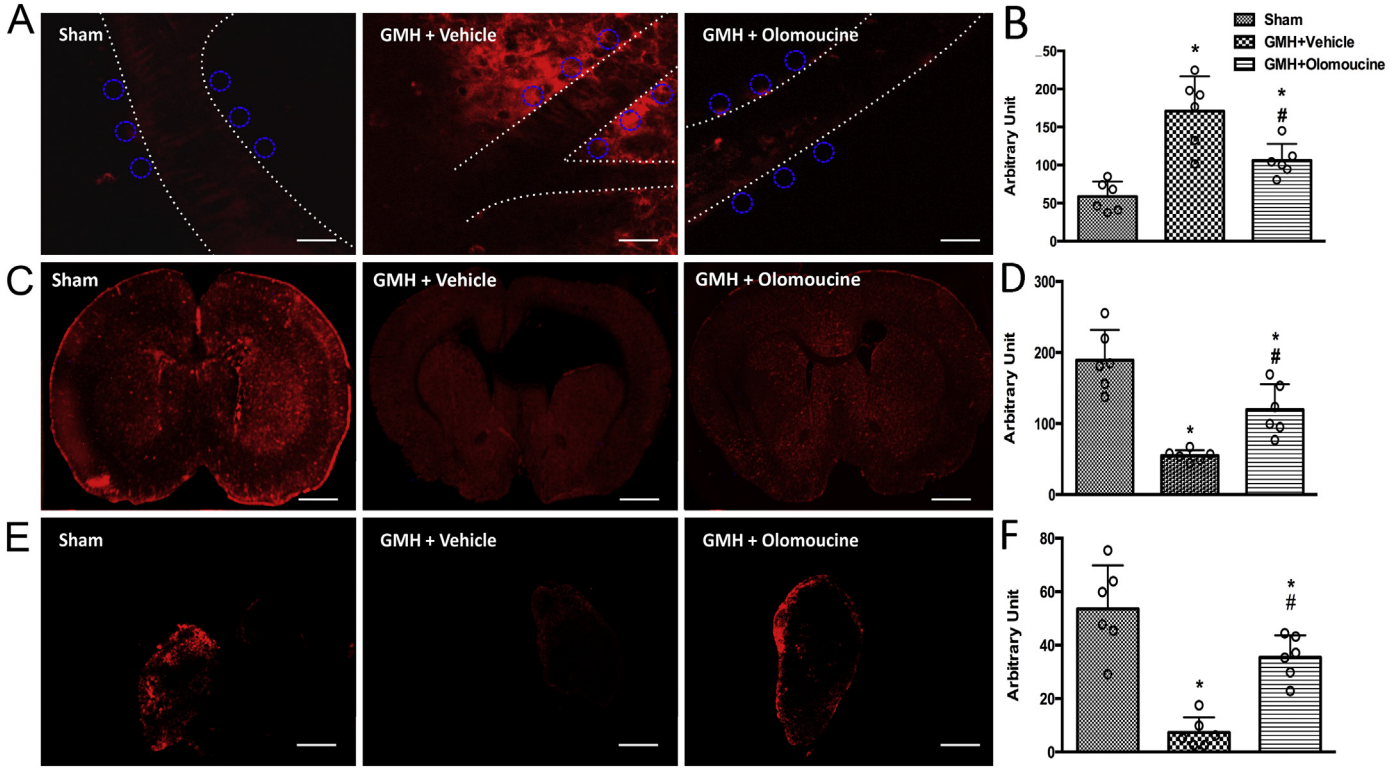

Fig. 4. GMH animals demonstrated impaired glymphatic function, as shown by decreased CSF-ISF exchange and reduced CSF reabsorption into the dcLNs while olomoucine treatment improved the glymphatic function at 28 days after GMH. A. Representative images of tracer-constituted CSF in the paravascular area. Scale bar = 40 μm. ROIs are demonstrated as circles. B. Quantitation of fluorescence intensity in the paravascular area. C. Representative images of tracer-constituted CSF throughout the whole coronal brain sections. Scale bar = 1.7 mm. D. Quantitation of fluorescence intensity throughout the brain. E. Representative images of dcLNs. Scale bar = 300 μm. F. Quantitation of fluorescence intensity inside the dcLNs. Values are expressed as mean ± SD. One-way ANOVA with Tukey's test. $^{*}P < .05$ compared with Sham, $^{\#}P < .05$ compared with GMH + Vehicle. N = 6.

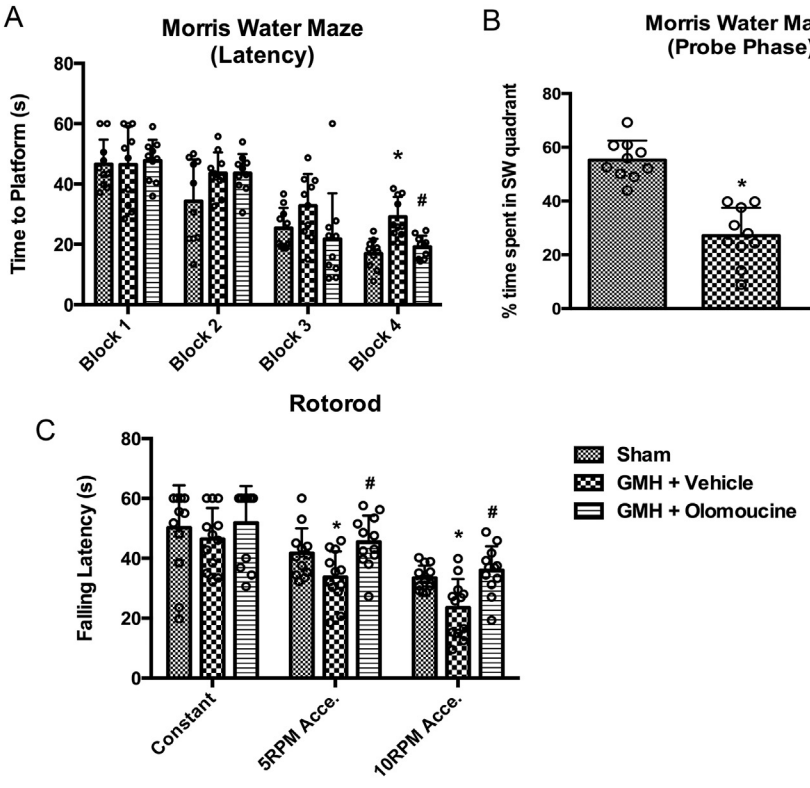

Fig. 5. Olomoucine improved long-term neurological outcomes between Day 22 and Day 27 after GMH. A. Swimming time to platform. N = 10. B. Percentage of time spent in the SW quadrant in the trial phase. N = 10. C. Falling latency in rotorod test. N = 12. Values are expressed as mean ± SD. Two-way ANOVA with Tukey's *post-hoc* test. $^{*}P < .05$ compared with Sham in the same category, $^{\#}P < .05$ compared with GMH + Vehicle in the same category.

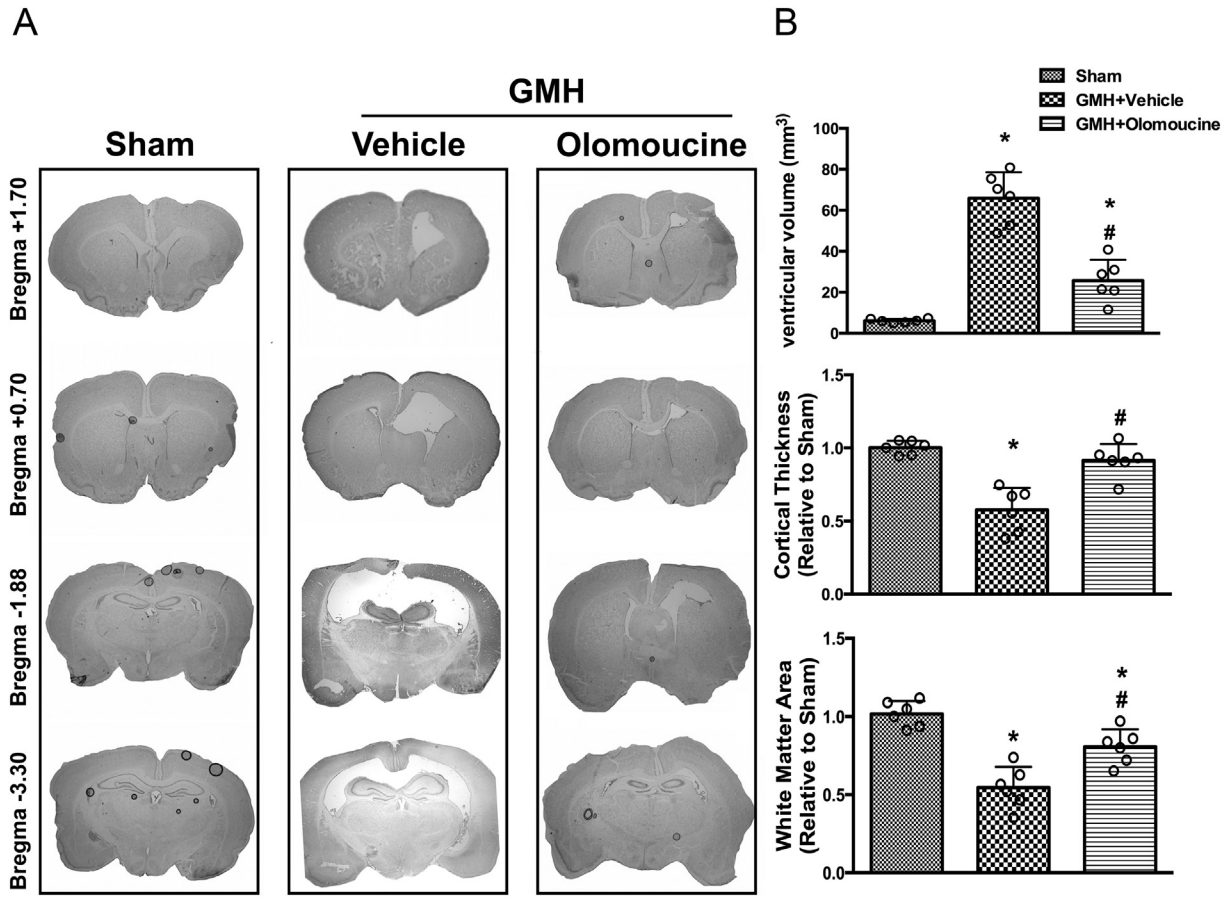

Fig. 6. Olomoucine ameliorated ventriculomegaly at 28 days after GMH. A. Representative Nissl-stained images at different locations relative to Bregma. B. Quantitation of ventricular volumes. C. Quantitation of cortical thickness relative to Sham. D. Quantitation of white matter area relative to Sham. Values are expressed as mean ± SD. One-way ANOVA with Tukey's *post-hoc* test. *P < .05 compared with Sham, #P < .05 compared with GMH + Vehicle. N = 6.

During this phase, Cyclin D1 and Cyclin E are the essential cyclins regulating cell cycle (Dimova and Dyson, 2005). We co-administered a SIRT1 inhibitor EX527 with olomoucine and isolated nuclear fraction of protein to test the expression profile of Rb and cyclins at 3 days after GMH. GMH significantly induced the phosphorylation of Rb and olomoucine attenuated this phosphorylation. In addition, GMH suppressed the expression of SIRT1 while olomoucine restored the SIRT1 level compared to vehicle-treated animals. Cyclin D1 and Cyclin E expression levels were also significantly higher after GMH and olomoucine effectively reduced the cyclins compared to GMH animals. These data were also in accordance with the GFAP and PCNA expression. However, EX527, a SIRT1 inhibitor, abolished the protective effects of olomoucine on SIRT1, restored Cyclin D1 level and had a tendency of restoring Cyclin E level, indicating that SIRT1 could be a potential downstream mediator in the anti-proliferative effect of olomoucine (Supplemental Fig. 4).

4. Discussion

GMH occurs in preterm infants and one of its common complications is post-hemorrhagic hydrocephalus. Current clinical management is surgical shunting, which is costly and can lead to numerous surgical complications. Thus, seeking pharmacological therapies to ameliorate hydrocephalus and/or to improve the prognosis of surgical shunting is of the utmost importance (Tang et al., 2016). Diuretics were once tested in clinical trials to attenuate neonatal PHH by inhibiting CSF production. However, data showed that they led to worse outcomes (Shooman et al., 2009). Thus, more attention has been drawn to the CSF reabsorption route in addition to inhibiting CSF overproduction (Del Bigio and Di Curzio, 2016; Karimy et al., 2017).

Although the brain was considered to be devoid of the lymphatics, emerging evidence shows that there is the glymphatic system which is responsible for transporting and eliminating wastes from the brain and that the meningeal lymphatic vessels, which connect with deep cervical lymph nodes, might function as the drainage in the downstream of the glymphatic system (Aspelund et al., 2015; Iliff and Nedergaard, 2013; Iliff et al., 2012; Louveau et al., 2015). Although there are controversies and skepticism about these new discoveries (Jin et al., 2016; Smith et al., 2017), the fact that subarachnoid villi are sparsely distributed in neonates makes it intriguing to investigators whether the glymphatic-meningeal lymphatic system plays a part in CSF reabsorption after neonatal PHH.

Immediately after GMH, the hematoma forms inside the ventricles and in the periventricular area, which obstructs the normal circulation of CSF (Garton et al., 2016). The current understanding is that the initial responses after GMH mainly involve degradation of blood clots, microglial phagocytosis of blood products, and then inflammatory responses following microglia activation(Garton et al., 2016; Strahle et al., 2014; Zhang et al., 2018). After the initial inflammatory response, microglia/macrophages would demonstrate the reparative phenotype and astrogliotic scar tissues start to form. In this study, we first established a treatment regimen of olomoucine that could effectively reduce astrocytic proliferation at three days after GMH. GFAP level remained upregulated up to 28 days post-ictus. This provides a time window to characterize the hydrocephalic event. A previous study from our laboratory shows that reduced astrogliosis was associated with attenuation of ventricular dilation (Manaenko et al., 2014). In addition, other studies showed that astrogliosis after brain injuries could perturb

the glymphatic system by altering AQP4 expression and polarity in adult animals (Iliff and Nedergaard, 2013; Wang et al., 2012). Thus we hypothesized that astrogliosis impairs CSF-ISF exchange through the glymphatic system in GMH animals, ultimately leading to reduced CSF drainage from the meningeal lymphatic system and into the dcLNs.

At 28 days after GMH, astrogliotic scarring was formed as indicated by increased number of periventricular astrocytes and GFAP expression in the whole brain. We expected that AQP4 level would also be increased with higher number of astrocytes since AQP4 is mostly expressed on astrocytes in the brain. Surprisingly, the overall AQP4 was not different between sham and GMH animals. We further categorized AQP4 as paravascular and stromal types. Immunofluorescence data suggested that paravascular AQP4 expression was significantly reduced while stromal AQP4 expression was higher in the vehicle-treated group. These findings would suggest that AQP4 is redistributed from the paravascular compartment to stromal areas. Since paravascular AQP4 functions as the rate-limiting mediator in the glymphatic system, this redistribution would likely lead to reduced CSF influx into the brain parenchyma. We observed that more tracer was confined within the paravascular region and proximal parenchyma and that CSF tracer diffusion throughout the whole brain in the coronal view was significantly lower in GMH animals. This CSF dynamics data is accordance with the AQP4 expression, which further suggests that glymphatic function was altered after GMH.

Olomoucine is a CDK inhibitor and has been shown to arrest cell cycle. Its inhibitory effect is not specific to a certain cell type and might have off-target effects on other cell types. However, it has been shown that it primarily targets cells that are proliferating at a higher rate than its physiological level (Di Giovanni et al., 2005; Tian et al., 2006). Considering astrocytes and microglia are proliferating faster than neurons after CNS injuries as the immune response, olomoucine might still provide more beneficial effects overall. Furthermore, some also suggested that olomoucine exerted anti-apoptotic effects on neurons (Di Giovanni et al., 2005). In addition, Park et al. showed that in primary culture of neonatal ganglionic neurons, olomoucine did not inhibit the normal growth, but rather promoted the survival of post-mitotic neurons (Park et al., 1996). We administered olomoucine to naïve animals and performed both short-term and long-term neurobehavioral tests. Our results showed that olomoucine alone did not alter the neurological outcomes compared to non-treated animals. These findings suggest that in neonates, olomoucine, at this treatment regimen, might not have much detrimental effect on normal cell growth, although the underlying mechanisms still remain largely unknown and more in vivo evidence is needed.

According to previous studies, CDK inhibitors are effective in inhibiting astrogliosis in various adult CNS injury models, including traumatic brain injury, spinal cord injury, etc. (Di Giovanni et al., 2005; Tian et al., 2006; Zhu et al., 2007). However, there are different properties of glial and immune cell in neonates compared to adults. For example, neonatal glial cells demonstrate greater plasticity and undergo less proliferation in response to brain injuries (Balasingam et al., 1994). Nevertheless, GMH elicits significant inflammatory response and consequent scar tissue formation up to 28 days after hemorrhage (Lekic et al., 2012; Manaenko et al., 2014). Interestingly, recent studies indicated that microglia and macrophages play a beneficial role in hematoma clearance after brain hemorrhage (Flores et al., 2016; Garton et al., 2017). We preliminarily demonstrated that olomoucine also inhibited the microglia/macrophage marker Iba-1 at 3 days after GMH (Supplemental Fig. 5). Moreover, neonatal microglia or macrophages have been shown to be more effective in facilitating hematoma clearance compared to those of adults (Agyemang et al., 2017; Mallard et al., 2019). Considering the great plasticity of the neonatal brains, it will be intriguing to assess whether or how olomoucine could affect this important function of neonatal microglia in the context of GMH and what overall benefits and side effects would CDK inhibitors bring.

Olomoucine inhibits CDKs, with the higher affinity to CDK2. CDK2 primarily facilitates the G1-S phase, featuring elevated levels of Cyclin D1 and Cyclin E. The underlying mechanism is that CDK2 inhibits the phosphorylation of Rb. The non-phosphorylated form of Rb, together with HDAC, arrests the cell cycle while the phosphorylated Rb recruits histone acetyltransferase (HAT) and facilitates the entry into the S phase for DNA replication. Thus, HATs and HDACs play regulatory roles in the G1-S phase (Dimova and Dyson, 2005). SIRT1 is an HDAC that regulates cell proliferation and has been characterized as a protective factor in the central nervous system (Herskovits and Guarente, 2014; Ng et al., 2015; Wan et al., 2018). Here we used the SIRT1 inhibitor EX527 to assess whether the beneficial effects of olomoucine would be abolished. Our data showed that Cyclin E and Cyclin D1 levels were partially restored with SIRT1 inhibition, indicating SIRT1 might be one of the HDACs in regulating the cell proliferation after GMH. However, whether other epigenetic modulating factors, such as histone methyltransferases, DNA memethyltransferases, also played a role in the astrocytic proliferation after GMH has not been tested in this current study. Considering the critical roles of these epigenetic factors in both ischemic and hemorrhagic strokes (Demyanenko et al., 2018; She et al., 2017; Sukumari-Ramesh et al., 2016), more investigation is warranted to thoroughly understand this astrogliosis mechanism.

There are a few limitations of this study. First, we only used one dextran tracer to characterize the CSF dynamics. Since the glymphatic system eliminates molecules of various weights, use of tracers of different molecular weights will further enhance our understanding of the glymphatic impairment in this scenario. Second, our data preliminarily demonstrated that olomoucine did not alter the neurobehavioral outcomes in naïve animals and that it had inhibitory effect on microglia/macrophage marker Iba-1. However, the effects of olomoucine on neurons and microglia need to be further addressed. We might need to investigate neuronal proliferation, apoptosis and regenerative capacity with the olomoucine treatment. In addition, pro- and anti-inflammatory factors, as well as hematoma resolution, need to be measured to assess the immune cell response with olomoucine treatment. Third, the amount of CSF reabsorption through the glymphatic-meningeal lymphtic system compared to the conventional subarachnoid villi route still remains to be determined. To quantify the amount of CSF reabsorption through the glymphatic –meningeal lymphatic vascular system as opposed to the conventional route, we might ligate the efferent lymphatic vessel of the dcLN as described and inject fluorescence tracer into the cisterna magna (Aspelund et al., 2015). Thus, we minimize the CSF absorption through the glymphatic-meningeal lymphatic system. We will collect the blood samples from internal jugular vein and quantify the fluorescent intensity from the plasma part, as an indicator of how much CSF is reabsorbed through the conventional route. We will then compare the ligation group to the non-ligation group. The difference between the two groups could be an indicator of how much CSF is reabsorbed through the glymphatic-meningeal lymphatic system.

5. Conclusions

Overall, this study is the first to characterize how the glymphatic system plays a role in post-hemorrhagic hydrocephalus in neonates. The impairment of the glymphatic system is associated with astrogliosis and redistribution of AQP4. Targeting astrogliosis might be a potential therapeutic strategy in ameliorating neonatal PHH.

Acknowledgments

Two-photon imaging was performed in the LLUSM Advanced Imaging and Microcopy Core with support of NSF Grant MRI-DBI 0923559 and the Loma Linda University School of Medicine.

The authors would like to thank Jay Malaguit and Dr. Weifeng Wan for their assistance in neurobehavioral tests. Authors would like to thank Jerry Flores for assistance in performing experiments.

This study was supported by R01 grant form National Institute of

Neurological Disorders and Stroke to JHZ (R01-NS078755) and a Research Award from the Hydrocephalus Association to YD.

Author contributions

Y.D. and T.Z. designed and performed the experiments, analyzed and interpreted the data and prepared the manuscript. G.W. performed intracisternal injections and participated in study design. D.M. assisted in two-photon imaging and revised the manuscript. D.K. conceived the study and troubleshooted the experiments. N.X. revised the manuscript. Y.Z. assisted in Western blot and short-term neurobehavioral studies. Q.L. assisted in long-term neurobehavioral studies. Y.D., D.M. and N.X. worked on the manuscript revision. J.T., and J.H.Z., participated in study design and coordinated the study.

Declaration of interest

Yan Ding is supported by a research award from Hydrocephalus Association.

Appendix A. Supplementary data

Supplementary data to this article can be found online at https://doi.org/10.1016/j.expneurol.2019.113003.

References

Agyemang, A.A., Sveinsdottir, K., Vallius, S., Sveinsdottir, S., Bruschettini, M., Romantsik, O., Hellstrom, A., Smith, L.E.H., Ohlsson, L., Holmqvist, B., Gram, M., Ley, D., 2017. Cerebellar exposure to cell-free hemoglobin following preterm intraventricular hemorrhage: causal in cerebellar damage? Transl. Stroke Res (ahead of print).

Aspelund, A., Antila, S., Proulx, S.T., Karlsen, T.V., Karaman, S., Detmar, M., Wiig, H., Alitalo, K., 2015. A dural lymphatic vascular system that drains brain interstitial fluid and macromolecules. J. Exp. Med. 212, 991–999.

Balasingam, V., Tejada-Berges, T., Wright, E., Bouckova, R., Yong, V.W., 1994. Reactive astrogliosis in the neonatal mouse brain and its modulation by cytokines. J. Neurosci. 14, 846–856.

Ballabh, P., 2010. Intraventricular hemorrhage in premature infants: mechanism of disease. Pediatr. Res. 67, 1–8.

Ballabh, P., Braun, A., Nedergaard, M., 2004. The blood-brain barrier: an overview: structure, regulation, and clinical implications. Neurobiol. Dis. 16, 1–13.

Del Bigio, M.R., Di Curzio, D.L., 2016. Nonsurgical therapy for hydrocephalus: a comprehensive and critical review. Fluids Barriers CNS 13, 3.

Demyanenko, S., Neginskaya, M., Berezhnaya, E., 2018. Expression of class I histone deacetylases in ipsilateral and contralateral hemispheres after the focal photothrombotic infarction in the mouse brain. Transl. Stroke Res. 9, 471–483.

Di Giovanni, S., Movsesyan, V., Ahmed, F., Cernak, I., Schinelli, S., Stoica, B., Faden, A.I., 2005. Cell cycle inhibition provides neuroprotection and reduces glial proliferation and scar formation after traumatic brain injury. Proc. Natl. Acad. Sci. U. S. A. 102, 8333–8338.

Dimova, D.K., Dyson, N.J., 2005. The E2F transcriptional network: old acquaintances with new faces. Oncogene 24, 2810–2826.

Feng, Z., Ye, L., Klebe, D., Ding, Y., Guo, Z.N., Flores, J.J., Yin, C., Tang, J., Zhang, J.H., 2017. Anti-inflammation conferred by stimulation of CD200R1 via Dok1 pathway in rat microglia after germinal matrix hemorrhage. J. Cereb. Blood Flow Metab. 39, 97–107 (271678X17725211).

Flores, J.J., Klebe, D., Rolland, W.B., Lekic, T., Krafft, P.R., Zhang, J.H., 2016. PPARgamma-induced upregulation of CD36 enhances hematoma resolution and attenuates long-term neurological deficits after germinal matrix hemorrhage in neonatal rats. Neurobiol. Dis. 87, 124–133.

Fukuda, A.M., Badaut, J., 2012. Aquaporin 4: a player in cerebral edema and neuroinflammation. J. Neuroinflammation 9, 279.

Garton, T., Keep, R.F., Wilkinson, D.A., Strahle, J.M., Hua, Y., Garton, H.J., Xi, G., 2016. Intraventricular hemorrhage: the role of blood components in secondary injury and hydrocephalus. Transl. Stroke Res. 7, 447–451.

Garton, T., Keep, R.F., Hua, Y., Xi, G., 2017. CD163, a hemoglobin/haptoglobin scavenger receptor, after intracerebral hemorrhage: functions in microglia/macrophages versus neurons. Transl. Stroke Res. 8, 612–616.

Herskovits, A.Z., Guarente, L., 2014. SIRT1 in neurodevelopment and brain senescence. Neuron 81, 471–483.

Iliff, J.J., Nedergaard, M., 2013. Is there a cerebral lymphatic system? Stroke 44, S93–S95.

Iliff, J.J., Wang, M., Liao, Y., Plogg, B.A., Peng, W., Gundersen, G.A., Benveniste, H., Vates, G.E., Deane, R., Goldman, S.A., Nagelhus, E.A., Nedergaard, M., 2012. A paravascular pathway facilitates CSF flow through the brain parenchyma and the clearance of interstitial solutes, including amyloid beta. Sci. Transl. Med. 4, 147ra111.

Jin, B.J., Smith, A.J., Verkman, A.S., 2016. Spatial model of convective solute transport in brain extracellular space does not support a “glymphatic” mechanism. J. Gen. Physiol. 148, 489–501.

Johnston, M., 2003. The importance of lymphatics in cerebrospinal fluid transport. Lymphat. Res. Biol. 1, 41–44 (discussion 45).

Karimy, J.K., Zhang, J., Kurland, D.B., Theriault, B.C., Duran, D., Stokum, J.A., Furey, C.G., Zhou, X., Mansuri, M.S., Montejo, J., Vera, A., DiLuna, M.L., Delpire, E., Alper, S.L., Gunel, M., Gerzanich, V., Medzhitov, R., Simard, J.M., Kahle, K.T., 2017. Inflammation-dependent cerebrospinal fluid hypersecretion by the choroid plexus epithelium in posthemorrhagic hydrocephalus. Nat. Med. 23, 997–1003.

Klebe, D., Krafft, P.R., Hoffmann, C., Lekic, T., Flores, J.J., Rolland, W., Zhang, J.H., 2014. Acute and delayed deferoxamine treatment attenuates long-term sequelae after germinal matrix hemorrhage in neonatal rats. Stroke 45, 2475–2479.

Lekic, T., Manaenko, A., Rolland, W., Krafft, P.R., Peters, R., Hartman, R.E., Altay, O., Tang, J., Zhang, J.H., 2012. Rodent neonatal germinal matrix hemorrhage mimics the human brain injury, neurological consequences, and post-hemorrhagic hydrocephalus. Exp. Neurol. 236, 69–78.

Louveau, A., Smirnov, I., Keyes, T.J., Eccles, J.D., Rouhani, S.J., Peske, J.D., Derecki, N.C., Castle, D., Mandell, J.W., Lee, K.S., Harris, T.H., Kipnis, J., 2015. Structural and functional features of central nervous system lymphatic vessels. Nature 523, 337–341.

Louveau, A., Plog, B.A., Antila, S., Alitalo, K., Nedergaard, M., Kipnis, J., 2017. Understanding the functions and relationships of the glymphatic system and meningeal lymphatics. J. Clin. Invest. 127, 3210–3219.

Lu, Z., Wang, Z., Yu, L., Ding, Y., Xu, Y., Xu, N., Li, R., Tang, J., Chen, G., Zhang, J.H., 2019. GCN2 reduces inflammation by p-eIF2alpha/ATF4 pathway after intracerebral hemorrhage in mice. Exp. Neurol. 313, 16–25.

Mallard, C., Tremblay, M.E., Vexler, Z.S., 2019. Microglia and neonatal brain injury. Neuroscience 405, 68–76.

Manaenko, A., Lekic, T., Barnhart, M., Hartman, R., Zhang, J.H., 2014. Inhibition of transforming growth factor-beta attenuates brain injury and neurological deficits in a rat model of germinal matrix hemorrhage. Stroke 45, 828–834.

Ng, F., Wijaya, L., Tang, B.L., 2015. SIRT1 in the brain-connections with aging-associated disorders and lifespan. Front. Cell. Neurosci. 9, 64.

Park, D.S., Farinelli, S.E., Greene, L.A., 1996. Inhibitors of cyclin-dependent kinases promote survival of post-mitotic neuronally differentiated PC12 cells and sympathetic neurons. J. Biol. Chem. 271, 8161–8169.

Raynaud, F.I., Whittaker, S.R., Fischer, P.M., McClue, S., Walton, M.I., Barrie, S.E., Garrett, M.D., Rogers, P., Clarke, S.J., Kelland, L.R., Valenti, M., Brunton, L., Eccles, S., Lane, D.P., Workman, P., 2005. In vitro and in vivo pharmacokinetic-pharmacodynamic relationships for the trisubstituted aminopurine cyclin-dependent kinase inhibitors olomoucine, bohemine and CYC202. Clin. Cancer Res. 11, 4875–4887.

She, D.T., Jo, D.G., Arumugam, T.V., 2017. Emerging roles of sirtuins in ischemic stroke. Transl. Stroke Res (ahead of print).

Shooman, D., Portess, H., Sparrow, O., 2009. A review of the current treatment methods for posthaemorrhagic hydrocephalus of infants. Cerebrospinal Fluid Res. 6 (1).

Smith, A.J., Yao, X., Dix, J.A., Jin, B.J., Verkman, A.S., 2017. Test of the ‘glymphatic’ hypothesis demonstrates diffusive and aquaporin-4-independent solute transport in rodent brain parenchyma. Elife 6.

Strahle, J.M., Garton, T., Bazzi, A.A., Kilaru, H., Garton, H.J., Maher, C.O., Muraszko, K.M., Keep, R.F., Xi, G., 2014. Role of hemoglobin and iron in hydrocephalus after neonatal intraventricular hemorrhage. Neurosurgery 75, 696–705 (discussion 706).

Sukumari-Ramesh, S., Alleyne Jr., C.H., Dhandapani, K.M., 2016. The histone deacetylase inhibitor suberoylanilide hydroxamic acid (SAHA) confers acute neuroprotection after intracerebral hemorrhage in mice. Transl. Stroke Res. 7, 141–148.

Sun, B.L., Wang, L.H., Yang, T., Sun, J.Y., Mao, L.L., Yang, M.F., Yuan, H., Colvin, R.A., Yang, X.Y., 2018. Lymphatic drainage system of the brain: a novel target for intervention of neurological diseases. Prog. Neurobiol. 163–164, 118–143.

Tang, J., Tao, Y., Jiang, B., Chen, Q., Hua, F., Zhang, J., Zhu, G., Chen, Z., 2016. Pharmacological preventions of brain injury following experimental germinal matrix hemorrhage: an up-to-date review. Transl. Stroke Res. 7, 20–32.

Tian, D.S., Yu, Z.Y., Xie, M.J., Bu, B.T., Witte, O.W., Wang, W., 2006. Suppression of astroglial scar formation and enhanced axonal regeneration associated with functional recovery in a spinal cord injury rat model by the cell cycle inhibitor olomoucine. J. Neurosci. Res. 84, 1053–1063.

Wan, W., Ding, Y., Xie, Z., Li, Q., Yan, F., Budbazar, E., Pearce, W.J., Hartman, R., Obenaus, A., Zhang, J.H., Jiang, Y., Tang, J., 2018. PDGFR-beta modulates vascular smooth muscle cell phenotype via IRF-9/SIRT-1/NF-kappaB pathway in subarachnoid hemorrhage rats. J. Cereb. Blood Flow Metab., 271678X18760954 (ahead of print).

Wang, M., Iliff, J.J., Liao, Y., Chen, M.J., Shinseki, M.S., Venkataraman, A., Cheung, J., Wang, W., Nedergaard, M., 2012. Cognitive deficits and delayed neuronal loss in a mouse model of multiple microinfarcts. J. Neurosci. 32, 17948–17960.

Yang, L., Kress, B.T., Weber, H.J., Thiyagarajan, M., Wang, B., Deane, R., Benveniste, H., Iliff, J.J., Nedergaard, M., 2013. Evaluating glymphatic pathway function utilizing clinically relevant intrathecal infusion of CSF tracer. J. Transl. Med. 11, 107.

Yu, J., Li, X., Matei, N., McBride, D., Tang, J., Yan, M., Zhang, J.H., 2018. Ezetimibe, a NPC1L1 inhibitor, attenuates neuronal apoptosis through AMPK dependent autophagy activation after MCAO in rats. Exp. Neurol. 307, 12–23.

Zador, Z., Stiver, S., Wang, V., Manley, G.T., 2009. Role of aquaporin-4 in cerebral edema and stroke. Handb. Exp. Pharmacol. 159–170.

Zakharov, A., Papaiconomou, C., Djenic, J., Midha, R., Johnston, M., 2003. Lymphatic cerebrospinal fluid absorption pathways in neonatal sheep revealed by subarachnoid injection of Microfil. Neuropathol. Appl. Neurobiol. 29, 563–573.

Zhang, Y., Xu, N., Ding, Y., Zhang, Y., Li, Q., Flores, J., Haghighiabyaneh, M., Doycheva, D., Tang, J., Zhang, J.H., 2018. Chemerin suppresses neuroinflammation and improves neurological recovery via CaMKK2/AMPK/Nrf2 pathway after germinal matrix hemorrhage in neonatal rats. Brain Behav. Immun. 70, 179–193.

Zhu, Z., Zhang, Q., Yu, Z., Zhang, L., Tian, D., Zhu, S., Bu, B., Xie, M., Wang, W., 2007. Inhibiting cell cycle progression reduces reactive astrogliosis initiated by scratch injury in vitro and by cerebral ischemia in vivo. Glia 55, 546–558.